Electronic Supplementary Material (ESI) for Inorganic Chemistry Frontiers.

Supporting Information

One-pot molten-salt constructing channels for holes transport and mass transfer over CoS_2 nanocubes for visible-light-driven CO_2 reduction

Fulin Wang,[⊥a] Man Zhou,[⊥b] Weiya Huang,[a] Kangqiang Lu,[a] Shaobo Ouayang,[a] Wentao Xiang,[a] Chensheng Zhou,[a] Changlin Yu,*[c] Kai Yang*[a]

a.School of Chemistry and Chemical Engineering, Jiangxi University of Science and Technology, Ganzhou 341000, Jiangxi, China.

b.School of Pharmaceutical Sciences, Gannan Medical University, Ganzhou 341000, Jiangxi, China.

c.School of Chemical Engineering, Key Laboratory of Petrochemical Pollution Process and Control, Guangdong Province, Guangdong University of Petrochemical Technology, Maoming 525000, Guangdong, China.

FuLin Wang and Man Zhou contributed equally to this work and were considered as co-first authors.

Experimental

Materials

Cobalt (II) nitrate hexahydrate ($Co(NO_3)_2 \cdot 6H_2O$), copper (II) nitrate trihydrate ($Cu(NO_3)_2 \cdot 3H_2O$), potassium thiocyanate (KSCN), tris (2,2′-bipyridyl) dichlororuthenium (II) hexahydrate ($C_{30}H_{24}Cl_2N_6Ru \cdot 6H_2O$) were purchased from Maclean's Biochemical Technology Co., Ltd. Triethanolamine ($C_6H_{15}NO_3$) and acetonitrile (CH_3CN) were purchased from Xilong Science Co., Ltd. All chemicals are used directly without further treatment.

Synthesis of CuSCN/CoS_2

The molten salt method was used to synthesize CuSCN-loaded CoS_2 photocatalysts. Specifically, $Co(NO_3)_2 \cdot 6H_2O$, $Cu(NO_3)_2 \cdot 3H_2O$, and KSCN mixed powders were ground evenly, then transferred to an alumina crucible and placed in a muffle furnace at 300 ℃ for 2 hours. The reaction products were collected, washed with deionized water, and finally dried under vacuum at 60 ℃ for 8 hours to obtain CuSCN/CoS_2 photocatalysts. During the preparation process, the loading capacities of CuSCN were adjusted by adjusting the amount of $Cu(NO_3)_2 \cdot 3H_2O$ added (the samples with a mass fraction of Cu element of 1%, 5%, and 10% were named 1-Cu/Co, 5-Cu/Co and 10-Cu/Co, respectively). For comparison, single component CoS_2 and CuSCN were prepared using the same method under the same conditions.

Characterizations

The crystal structure was determined by X-ray diffraction (XRD, Bruker D8, Cu Kα, λ= 0.15406 nm). Morphological characteristics were measured by scanning electron microscopy (SEM, ZEISS Sigma 500). The structure and elemental distribution of the prepared samples were evaluated by transmission electron microscopy (TEM, JEOL JEM-2100 F) and energy dispersive X-ray spectroscopy (EDX). In-situ X-ray photoelectron spectroscopy (XPS) in the dark and under

light irradiation for 15 min was measured on X-ray photoelectron spectra (Nexsa, Al K Alpha). The optical absorption characteristics of the samples were investigated by UV-visible diffuse reflectance spectroscopy (DRS, UV-2600, Shimadzu) using the $BaSO_4$ reference standard. The Fourier transform infrared spectra (FTIR) were collected by the Nicolet 5700 FT-IR spectrometer using KBr pellets as reference. Nitrogen adsorption-desorption isotherms and CO_2 adsorption capacity for samples were analyzed using ASAP 2020 automatic analyzer. The photoluminescence (PL, F-4600) spectroscopy was measured to expose the reintegration of electron-hole pairs. CO_2 temperature programmed desorption (TPD) was carried out via an automatic chemical adsorption apparatus (AutoChem II 2920). In-situ FTIR spectra were collected using a Perkin Elmer Spectrum. Photoelectric chemical measurements were carried out in a three-electrode system on an electrochemical workstation (CHI660E), Ag/AgCl as reference electrode and Pt line as counter electrode. Indium tin oxide conductive glass (ITO) was used as the working electrode (10 mg sample was dissolved in 3 drops of ethanol, including 10 μL Nafion solution, and then the solution was subjected to ultrasonic for 40 min to completely disperse the sample, and the loading effective area was 0.25 cm^2).

Photocatalytic CO_2 reduction

In a typical reaction, 30 mg of photocatalyst, 5mg of tris (2,2′-bipyridyl) dichlororuthenium (II) hexahydrate, 3 mL of acetonitrile, 2 mL of deionized water, and 1 mL of triethanolamine were added to a 50 mL quartz reactor. Then, the reactor was purged with high-purity CO_2 gas at 1 atm pressure for 30 min. An Xe lamp with a 420 nm filter serves as the light source. After 2 hours of light reaction, CO, H_2, and CH_4 were detected by gas chromatography equipped with TCD and FID. The selectivity S(CO) of CO was calculated by the following formula:

$$\mathrm{S(CO)} = \frac{X(CO)}{X(CO) + X(H_2) + X(CH_4)} \times 100\%$$

where X(CO), X(H_2) and X(CH_4) were the yields of CO, H_2 and CH_4 after the reaction, respectively.

Computational details

All DFT calculation were constructed and implemented in the Vienna ab initio simulation package (VASP).[1,2] Using the electron exchange and correlation energy was treated within the generalized gradient approximation in the Perdew−Burke−Ernzerhof functional (GGA-PBE),[3] the calculations were done with a plane-wave basis set defined by a kinetic energy cutoff of 450 eV. The long-range dispersion interactions between adsorbates and surface was treated applying DFT-D3 method developed by grimme et al.[4] The k-point sampling was obtained from the Monkhorst−Pack scheme with a (3 × 3 × 1) mesh for optimization and electronic structure. The geometry optimization and energy calculation are finished when the electronic self-consistent iteration and force were reach 10^{-5} eV and 0.02 eV $Å^{-1}$, respectively. Transition states (TSs) were located with a constrained minimisation technique converged to 0.05 eV eV $Å^{-1}$.[5]

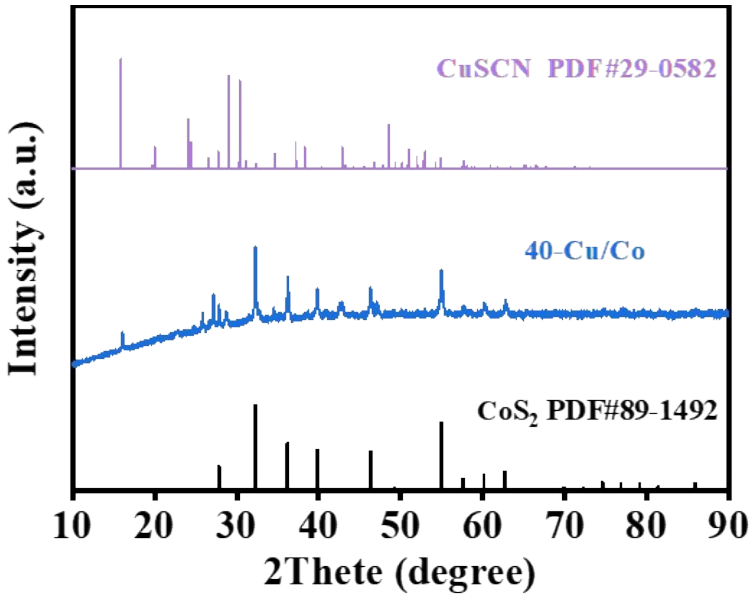

Fig. S1 XRD diagram of 40-Cu/Co.

(a)

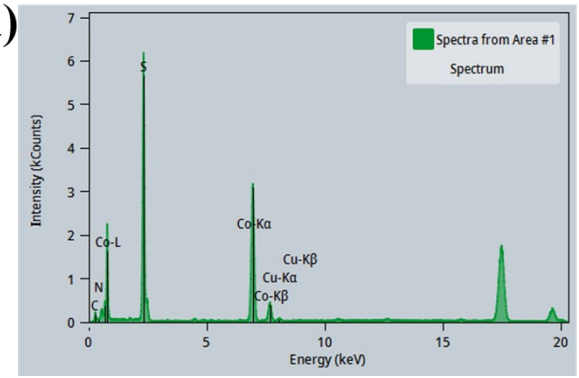

(b)

Element	Atomic Fraction (%)	Mass Fraction (%)
C	5.09	1.49
N	1.16	0.40
S	56.28	44.09
Co	36.76	52.93
Cu	0.71	1.09

Fig. S2 (a) EDX spectrum and (b) percentage of each element of 1-Cu/Co.

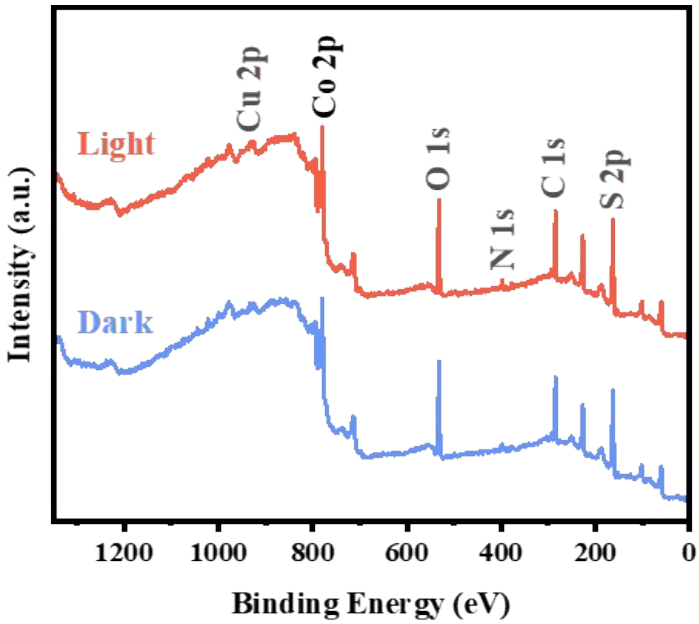

Fig. S3 *In situ* XPS spectra of 1-Cu/Co: full spectrum.

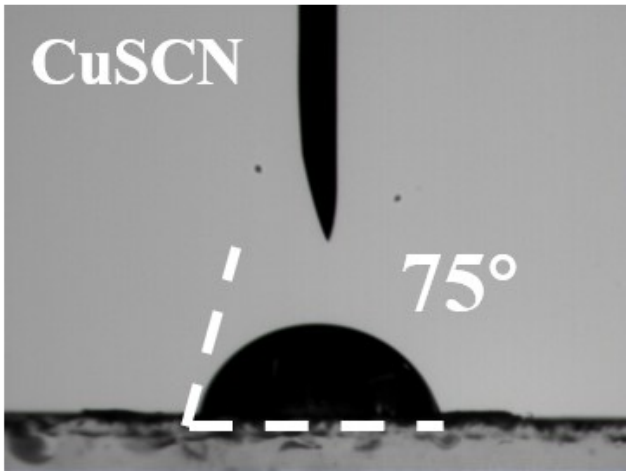

Fig. S4 Contact angle between CuSCN and H_2O.

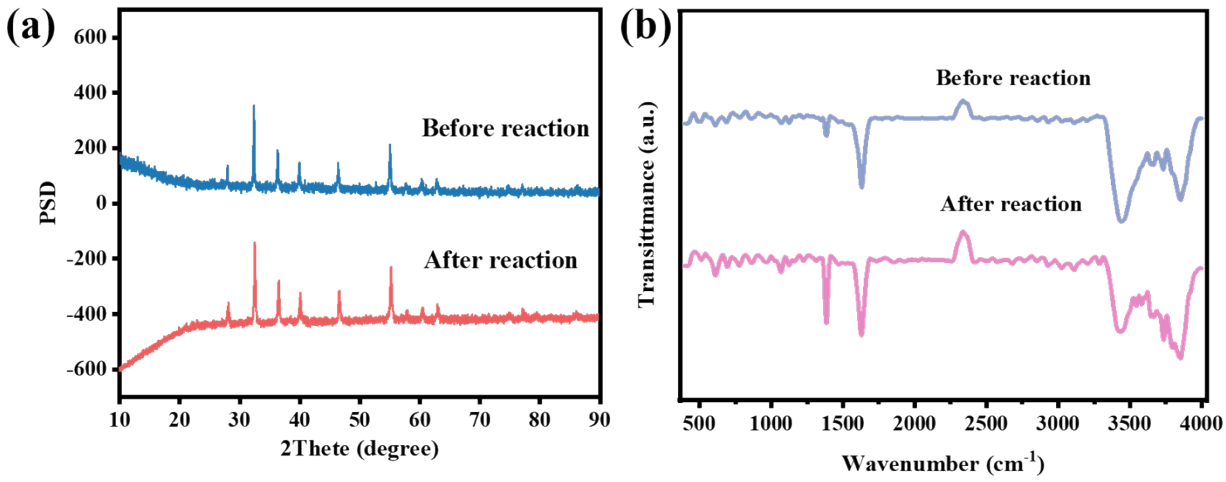

Fig. S5 XRD patterns (a) and FT-IR spectrums (b) before and after reaction of 1-Cu/Co.

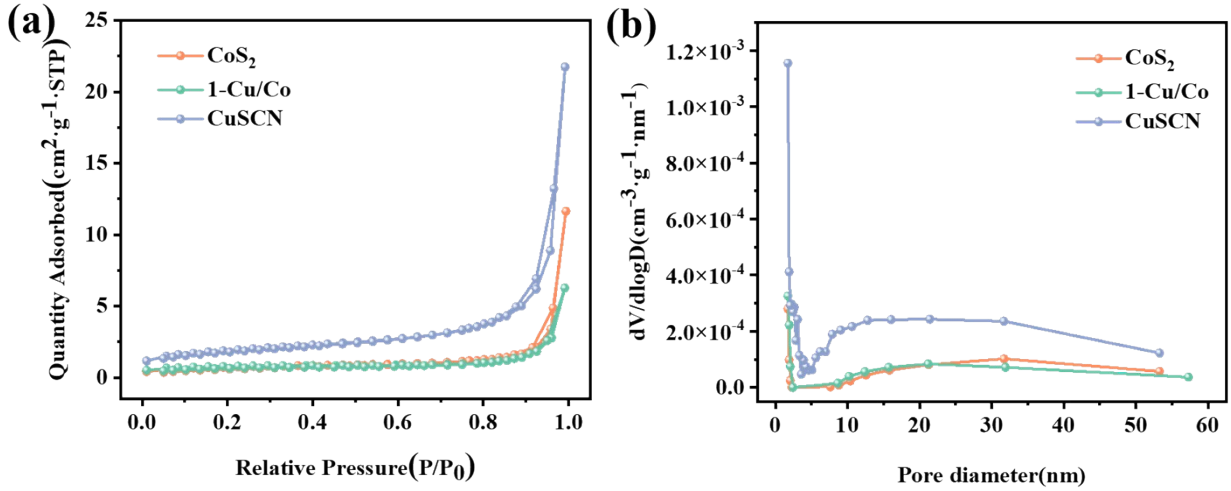

Fig. S6 (a) N_2 adsorption-desorption plots. (b) The corresponding BJH pore size distributions.

Table S1 Specific surface area, pore volume and average pore diameter of samples.

Samples	Specific surface area (m^2/g)	Pore volume (cm^3/g)	Average pore diameter (nm)
CoS2	2.4803	0.0180	36.6711
1-Cu/Co	2.5566	0.0097	26.6079
CuSCN	6.4924	0.0327	26.2910

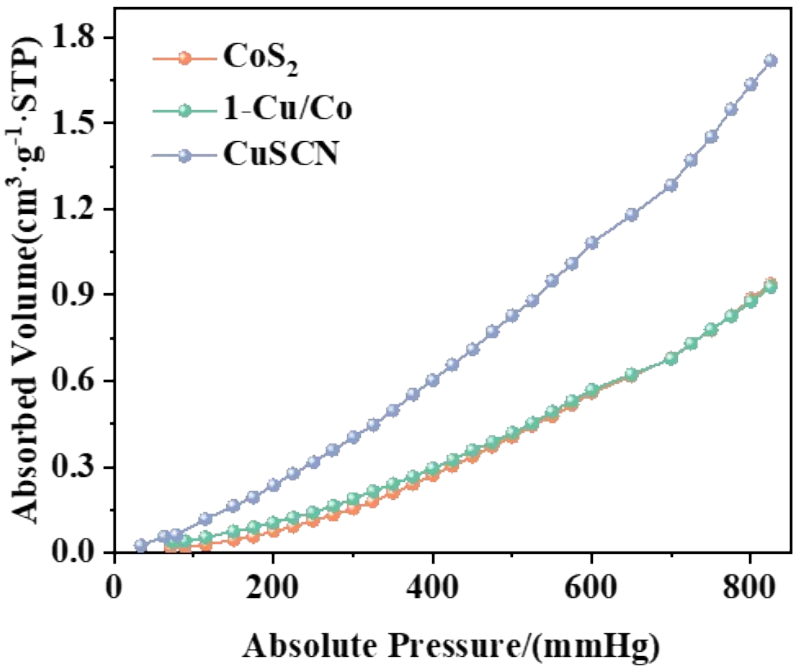

Fig. S7 CO_2 adsorption isotherms.

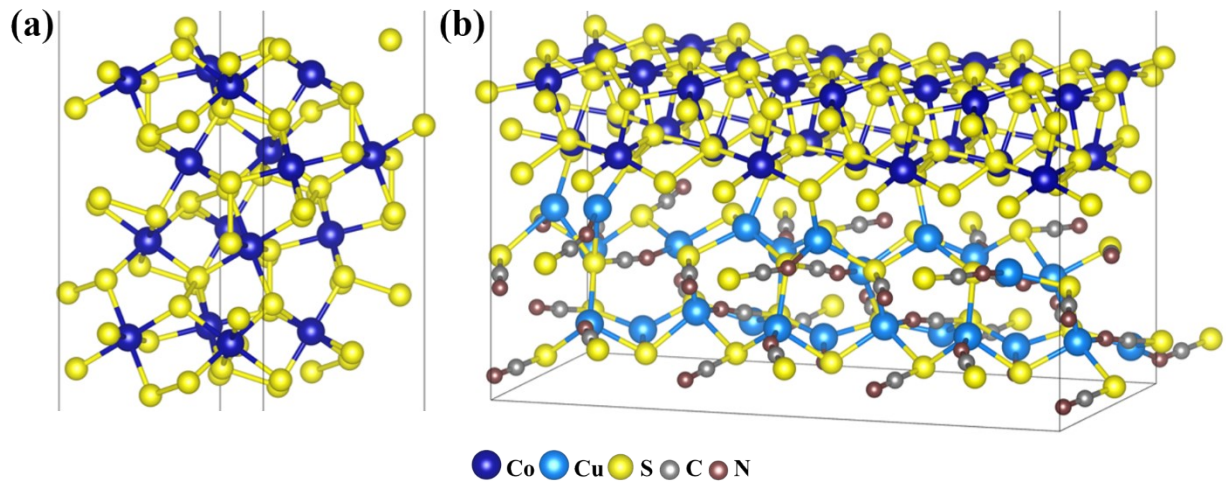

Fig. S8 Theoretical models of (a) CoS_2 and (b) $CuSCN/CoS_2$.

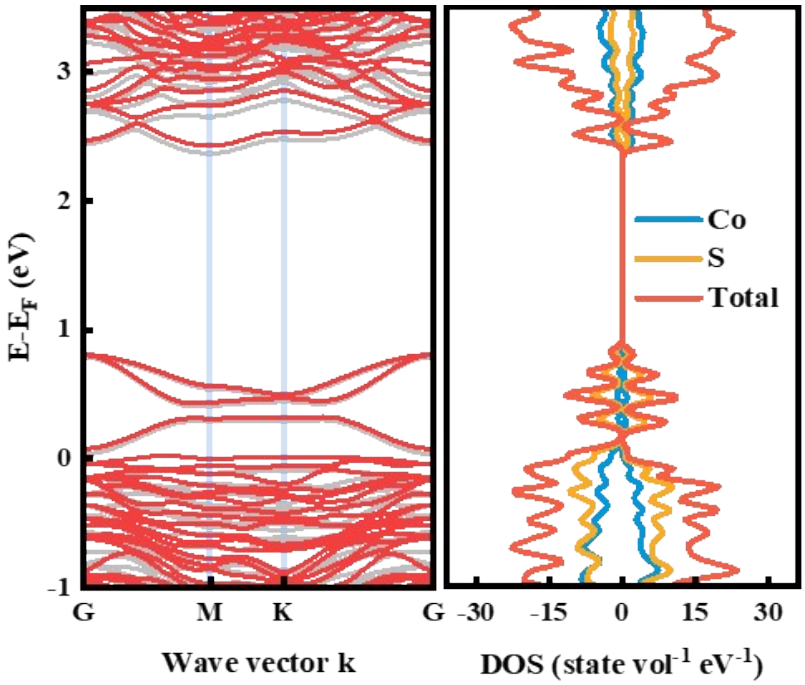

Figu. S9 Calculated electronic band structure (gray indicates spin up state, red indicates spin down state) and state density of CoS_2.

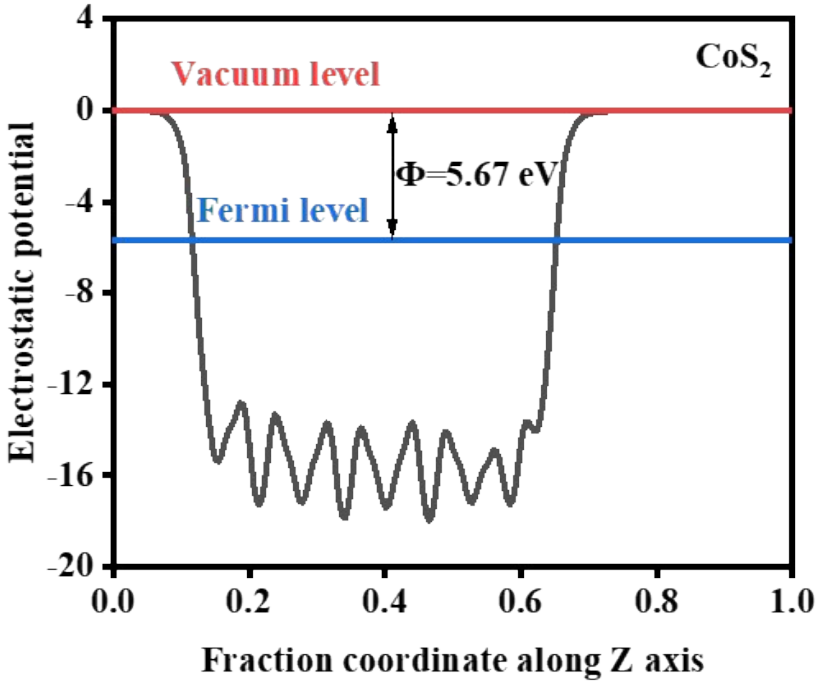

Fig. S10 Work functions of CoS_2.

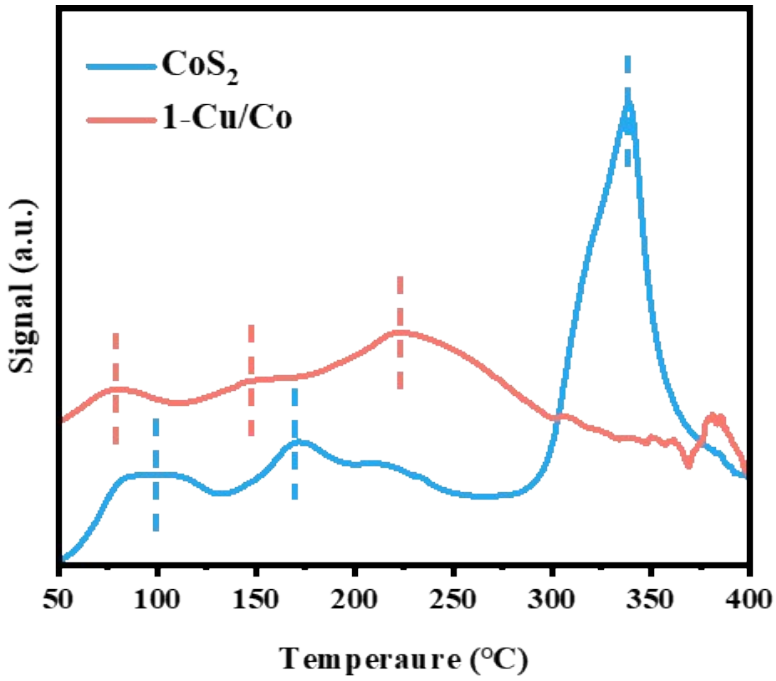

Fig. S11 CO_2-TPD diagram.

Table S2 Comparison of photocatalytic performance for CO_2 conversion to CO

Photocatalyst	Reductant	Light source	CO production rate (μmol/g/h)	Ref.
DA-CTF	H_2O, MeCN, TEOA, $Ru(bpy)_3^{2+}$	300W Xe lamp $\lambda \geq 420$ nm	155.0	6
$CuInS_4/In_2S_3$	H_2O, MeCN, TEOA, $Co(bpy)_3^{2+}$	300W Xe lamp	19.0	7
Cu_2O/MnO_x	H_2O, $KHCO_3$, Na_2SO_3	300W Xe lamp $\lambda \geq 420$ nm	114.4	8
CoO_x/MIL-101(Cr)	H_2O, MeCN, TEOA, $Ru(bpy)_3^{2+}$	300W Xe lamp	28.7	9
Co-$CuInS_2$	H_2O	300W Xe lamp	15.2	10
Co/C	H_2O, MeCN, TEOA, $Ru(bpy)_3^{2+}$	300W Xe lamp $\lambda \geq 420$ nm	172.1	11
Cu-ZnS	H_2O, Chloroform, 2-propanol	300W Xe lamp	68.9	12
Co-Bi_3O_4Br	H_2O	300W Xe lamp	107.1	13
Cu/In_2O_3/C	H_2O, MeCN, TEA	300W Xe lamp	43.7	14
CdS/BCN	H_2O, MeCN, TEOA, $Co(bpy)_3^{2+}$	300W Xe lamp $\lambda \geq 420$ nm	250.0	15
Co_9S_8@$ZnIn_2S_4$/CdS	H_2O, MeCN, Na_2SO_3	300W Xe lamp	82.1	16
Co-dca	H_2O, MeCN, TEOA, $Ru(bpy)_3^{2+}$	300W Xe lamp $\lambda \geq 420$ nm	254.0	17
1-Cu/Co	**H_2O, MeCN, TEOA, $Ru(bpy)_3^{2+}$**	**300W Xe lamp $\lambda \geq 420$ nm**	**289.8**	**This work**

Table S3 Gibbs free energy for each step.

Steps \ Photocatalysts	CoS_2	CuSCN	CuSCN/CoS_2 (Co sites)	CuSCN/CoS_2 (Cu sites)
* → *CO_2 (G1)	0.07 eV	0.02 eV	-0.02 eV	0.05 eV
*CO_2 → *COOH (G2)	0.69 eV	0.78 eV	0.22 eV	0.90 eV
*COOH → *CO (G3)	0.42 eV	-0.91 eV	0.67 eV	-0.85 eV
*CO → * + CO (G4)	-0.57 eV	0.71 eV	-0.27 eV	0.50 eV

References

1 G. Kresse and J. Furthmüller, Efficiency of Ab-Initio Total Energy Calculations for Metals and Semiconductors Using a Plane-Wave Basis Set, *Comput. Mater. Sci.*, 1996, **6**, 15–50.

2 G. Kresse and J. Furthmüller, Efficient Iterative Schemes for *Ab Initio* Total-Energy Calculations Using a Plane-Wave Basis Set, *Phys. Rev. B*, 1996, **54**, 11169–11186.

3 M. Ernzerhof and J. P. Perdew, Generalized Gradient Approximation to the Angle- and System-Averaged Exchange Hole, *J. Chem. Phys.*, 1998, **109**, 3313–3320.

4 S. Grimme, J. Antony, S. Ehrlich and H. Krieg, A Consistent and Accurate *Ab Initio* Parametrization of Density Functional Dispersion Correction (DFT-D) for the 94 Elements H-Pu, *J. Chem. Phys.*, 2010, **132**, 154104.

5 A. Michaelides, Z.-P. Liu, C. J. Zhang, A. Alavi, D. A. King and P. Hu, Identification of General Linear Relationships between Activation Energies and Enthalpy Changes for Dissociation Reactions at Surfaces, *J. Am. Chem. Soc.*, 2003, **125**, 3704–3705.

6 S. Sadigh Akbari and F. Karadas, Selective Photocatalytic CO_2 Reduction by Cobalt Dicyanamide, *Dalton Trans.*, 2022, **51**, 12569–12575.

7 J. Yang, X. Zhu, Z. Mo, J. Yi, J. Yan, J. Deng, Y. Xu, Y. She, J. Qian, H. Xu and H. Li, A Multidimensional In_2S_3–$CuInS_2$ Heterostructure for Photocatalytic Carbon Dioxide Reduction, *Inorg. Chem. Front.*, 2018, **5**, 3163–3169.

8 H. Huo, D. Liu, H. Feng, Z. Tian, X. Liu and A. Li, Double-Shelled Cu_2O/MnO_x Mesoporous Hollow Structure for CO_2 Photoreduction with Enhanced Stability and Activity, *Nanoscale*, 2020, **12**, 13912–13917.

9 Y. Ma, J. Du, Y. Fang and X. Wang, Encapsulation of Cobalt Oxide into Metal-Organic Frameworks for an Improved Photocatalytic CO_2 Reduction, *ChemSusChem*, 2021, **14**, 946–951.

10 Z. Yang, J. Yang, H. Ji, M. He, Y. Song, W. Zhang, J. Yuan, X. She, Y. She, H. Li and H. Xu, Construction of S-Co-S Internal Electron Transport Bridges in Co-Doped $CuInS_2$ for Enhancing Photocatalytic CO_2 Reduction, *Mater. Today Chem.*, 2022, **26**, 101078.

11 K. Zhao, S. Zhao, C. Gao, J. Qi, H. Yin, D. Wei, M. F. Mideksa, X. Wang, Y. Gao, Z. Tang and R. Yu, Metallic Cobalt–Carbon Composite as Recyclable and Robust Magnetic Photocatalyst for Efficient CO_2 Reduction, *Small*, 2018, **14**, 1800762.

12 X. Zhang, D. Kim and L. Y. S. Lee, Copper-Doped ZnS with Internal Phase Junctions for Highly Selective CO Production from CO_2 Photoreduction, *ACS Appl. Energy Mater.*, 2021, **4**, 2586–2592.

13 M. Kunitski, N. Eicke, P. Huber, J. Köhler, S. Zeller, J. Voigtsberger, N. Schlott, K. Henrichs, H. Sann, F. Trinter, L. Ph. H. Schmidt, A. Kalinin, M. S. Schöffler, T. Jahnke, M. Lein and R. Dörner, Double-Slit Photoelectron Interference in Strong-Field Ionization of the Neon Dimer, *Nat. Commun.*, 2019, **10**, 1.

14 A. Zhou, C. Zhao, J. Zhou, Y. Dou, J.-R. Li and M. Wei, Tailoring the Electronic Structure of In_2O_3/C Photocatalysts for Enhanced CO_2 Reduction, *J. Mater. Chem. A*, 2023, **11**, 12950–12957.

15 M. Zhou, S. Wang, P. Yang, C. Huang and X. Wang, Boron Carbon Nitride Semiconductors Decorated with CdS Nanoparticles for Photocatalytic Reduction of CO_2, *ACS Catal.*, 2018, **8**, 4928–4936.

16 Y. Zhang, Y. Wu, L. Wan, H. Ding, H. Li, X. Wang and W. Zhang, Hollow Core–Shell Co_9S_8@$ZnIn_2S_4$/CdS Nanoreactor for Efficient Photothermal Effect and CO_2 Photoreduction, *Appl. Catal. B Environ.*, 2022, **311**, 121255.
17 S. Sadigh Akbari and F. Karadas, Selective Photocatalytic CO_2 Reduction by Cobalt Dicyanamide, *Dalton Trans.*, 2022, **51**, 12569–12575.